Chemical Science

EDGE ARTICLE

View Article Online
View Journal | View Issue

Cite this: *Chem. Sci.*, 2015, **6**, 6841

Visualizing changes in mitochondrial Mg^{2+} during apoptosis with organelle-targeted triazole-based ratiometric fluorescent sensors†

G. Zhang, J. J. Gruskos, M. S. Afzal and D. Buccella*

Received 7th July 2015
Accepted 15th October 2015

DOI: 10.1039/c5sc02442k

www.rsc.org/chemicalscience

Magnesium is one of the most abundant metals in cells and is essential for a wide range of cellular processes. Magnesium imbalance has been linked to a variety of diseases, but the scarcity of sensors suitable for detection of Mg^{2+} with subcellular resolution has hampered the study of compartmentalization and mobilization of this ion in the context of physiological and pathological processes. We report herein a family of fluorescent probes for targeted detection of free Mg^{2+} in specific intracellular organelles, and its application in the study of programmed cell death. The new sensors feature a triazole unit that plays both structural and electronic roles by serving as an attachment group for targeting moieties, and modulating a possible internal charge transfer process for ratiometric ion sensing. A probe decorated with an alkylphosphonium group was employed for the detection of mitochondrial Mg^{2+} in live HeLa cells, providing the first direct observation of an increase in free Mg^{2+} levels in this organelle in the early stages of Staurosporine-induced apoptosis.

Introduction

Magnesium is essential for numerous cellular processes, playing a role in activation of enzymes, structural stabilization of nucleic acids and proteins, modulation of ion channels, and as a second messenger.[1,2] In mammalian cells, Mg^{2+} is the most abundant divalent cation, with a total concentration typically maintained in the mid-millimolar range in most cell types.[3,4] Abnormal levels of serum or cellular magnesium have been linked to various conditions including cardiovascular disease, diabetes, neurodegeneration, and cancer.[5–9]

Despite the importance of Mg^{2+} homeostasis in human health, details of the mechanisms that regulate the concentration of this ion at the cellular and subcellular level have remained partially obscure, primarily due to the paucity of efficient tools for the measurement of Mg^{2+} with the required spatial and temporal resolutions.[10] In particular, the ability to study intracellular ion distribution and mobilization between subcellular domains has been hampered by the scarcity of probes capable of reporting organelle-specific levels of Mg^{2+}. In this regard, Oka and coworkers developed a rosamine-based Mg^{2+} turn-on indicator that spontaneously localizes to mitochondria.[11] More recently, the same group reported a related turn-on biarsenical dye that can be anchored to tetracysteine-tagged proteins expressed in specific compartments, thus enabling the visualization of Mg^{2+} dynamics upon mitochondrial membrane depolarization.[12] Genetically encoded protein-based FRET fluorescent sensors reported by Merkx and coworkers have been targeted to other intracellular compartments.[13] A general platform suitable for organelle-targeted ratiometric detection of Mg^{2+} with small-molecule indicators, however, is still lacking.

The activation of apoptotic pathways bears close connection with cellular homeostasis of divalent cations, with Ca^{2+} playing a major role in regulation of the intrinsic (mitochondrial) pathway.[14–16] The role of Mg^{2+}, on the other hand, has not been clearly established. Changes in cytosolic Mg^{2+} concentration have been observed in glycodeoxycolate-induced apoptosis of hepatocytes,[17] during proanthocyanidin/doxorubicin-induced apoptosis in K562/DOX cells,[18] and in Fas ligand-induced apoptosis of B lymphocytes.[19] In the latter example, an increase in cytosolic free Mg^{2+} was found to be independent of the extracellular concentration of the metal, which led to the hypothesis that mitochondria could be acting as an intracellular source. Until now, however, the dynamics of mitochondrial Mg^{2+} during apoptosis have not been observed directly in whole cells. In this report, we introduce a new family of fluorescent sensors for targeted ratiometric detection of Mg^{2+} in organelles of interest (Fig. 1), and present the first direct observation of the changes in free Mg^{2+} levels in mitochondria during early stages of Staurosporine-induced apoptosis in HeLa cells.

Department of Chemistry, New York University, New York 10003, USA. E-mail: dbuccella@nyu.edu

† Electronic supplementary information (ESI) available: Experimental details, metal selectivity plots, determination of apparent dissociation constants, fluorescence microscopy co-localization analysis, and supporting figures. See DOI: 10.1039/c5sc02442k

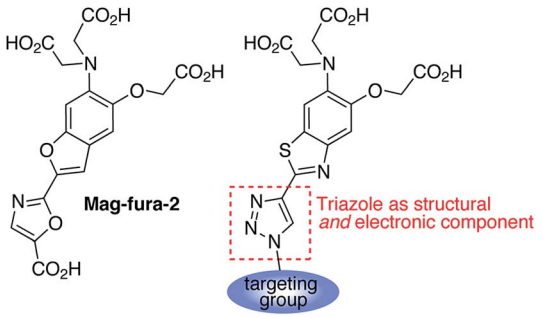

Fig. 1 Design of triazole-based ratiometric sensors for targeted intracellular Mg^{2+} detection.

Results and discussion

Sensor design and synthesis

1,2,3-Triazoles assembled by copper catalyzed alkyne–azide cycloaddition (CuAAC)[20] have been used extensively as structural linkages in fluorophore biocojugation, but only recently have their electronic features been exploited to influence the properties of fluorescent labels and sensors.[21] We envisioned a sensor design incorporating a 1,2,3-triazole moiety as part of the fluorophore, replacing the oxazole group in furaptra[22] and related 'fura' dyes.[23] The triazole is thus intended to serve a dual purpose, namely, a structural role as an attachment group between fluorophore and an organelle-targeting moiety, and a possible electronic role as a modulator of an internal charge transfer (ICT) process for fluorescence-based ion sensing.

We synthesized an alkynyl-functionalized benzothiazole, **5**, to be employed as a precursor for rapid assembly of targeted ratiometric sensors *via* CuAAC (Scheme 1). This compound was obtained from 2-aminobenzothiazole **2**, which was prepared by modification of a protocol reported by Metten and coworkers.[24] The amino function was converted by diazotization and treatment with potassium iodide, followed by Sonogashira coupling with trimethylsilylacetylene and subsequent deprotection. The late stage click reaction with the resulting alkyne may be used to tune the chemical and biological properties of the final sensors with minimum synthetic effort, based on sensible choice of azide.

With the goal of evaluating the performance of our sensor design, model sensors **7a** and **7b** were prepared by reaction of alkyne **5** with benzyl- and phenylazide, respectively, followed by ester hydrolysis. Cycloaddition was performed on the ester-protected sensors in order to minimize residual copper binding to the metal-recognition unit, which may interfere with metal sensing in subsequent studies.

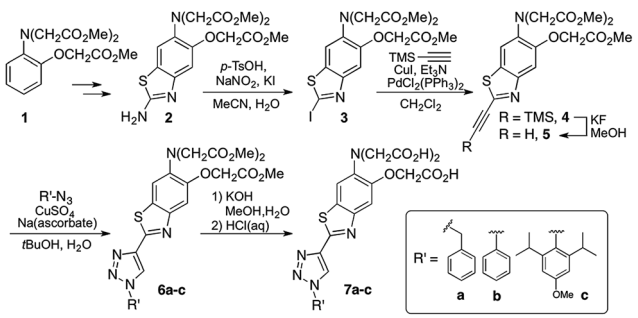

Scheme 1 Synthesis of triazole-containing sensors.

Spectroscopic properties of fluorescent sensors

Photophysical characterization of sensors **7a,b** was conducted in aqueous buffer mimicking physiological ionic strength (Table 1). The new triazole-based probes show large Stokes shifts in aqueous solution, and respond to Mg^{2+} with a significant blue shift in the fluorescence excitation and emission maxima (Table 1 and Fig. 2). These observations are consistent with a destabilizing effect of the cation on an excited state characterized by a large dipole moment. A similar response is observed with the related furaptra (Mag-fura-2) dye,[22] suggesting a common ICT mechanism with the nitrogen of the metal-recognition unit acting as a donor.[25] This notion is currently being investigated computationally.

Both benzyl and phenyl derivatives **7a** and **7b** exhibit similar absorption and fluorescence emission wavelengths in their metal-free and -bound forms (Table 1), but the phenyl derivative exhibits a lower quantum yield than the benzyl derivative, well below 10%. We postulated that rotation around the triazole-phenyl bond may provide an efficient non-radiative decay pathway for **7b**, *via* distortion of the excited state[26] and/or access to a non-emissive twisted intramolecular charge transfer state.[27] Attempts to test this hypothesis through measurements in solvents of increasing viscosity proved inconclusive. However, incorporation of sterically demanding isopropyl substituents on the *ortho* position of the phenyl ring (see derivative **7c**, Scheme 1), which increase the barrier of rotation and disrupt a possible coplanar arrangement of phenyl and triazole rings, resulted in the recovery of the fluorescence quantum yields to values comparable to those of benzyl derivative **7a**.

Compounds **7a** and **7c** are useful for ratiometric detection of Mg^{2+} (Fig. 2 and S1–S3, ESI†), with apparent dissociation constants in the low millimolar range at 25 °C ($K_{d,Mg^{2+}} = 8.8 \pm 0.4$ and 9.5 ± 0.4 mM for **7a** and **7c**, respectively). On the other hand, the difference in brightness for the metal-free and -bound forms of phenyl derivative **7b** makes it more suitable for a turn-on application (~13-fold turn-on, $K_{d,Mg^{2+}} = 7.8 \pm 0.2$ mM). It is important to note that these indicators detect *free* Mg^{2+}, and do not respond to bound forms of the ion such as MgATP. In this regard, the fluorescence response of a solution of compound **7c** treated with increasing amounts of Mg^{2+} in the presence of 18.4 mM ATP (Fig. S5†) can be modelled by considering a single binding event for the complexation of Mg^{2+} by the sensor. The fluorescence ratio expressed as a function of $[Mg^{2+}]_{free}$, calculated from the amount of total magnesium and dissociation of MgATP ($K_d = 50$ μM (ref. 30)), matches the isotherms obtained in the absence of the ATP (Fig. S5B†).

The optical properties of derivatives **7a–c** were also tested in the presence of high concentrations of other biologically relevant divalent metal ions, including Ca^{2+}, Mn^{2+}, Fe^{2+}, Co^{2+}, Ni^{2+}, Cu^{2+}, and Zn^{2+} (Fig. S6–S8†). The metal selectivity of the

Table 1 Photophysical properties of model compounds **7a–c** and **Mag-*mito*** sensor[a]

	Absorption λ_{max} (nm), $\varepsilon \times 10^3$ (M^{-1} cm^{-1})		Excitation λ_{max} (nm)		Emission λ_{max} (nm), Φ^b				
	Unbound	Mg^{2+}-saturated	Unbound	Mg^{2+}-saturated	Unbound	Mg^{2+}-saturated	R_{max}/R_{min}	$K_{d,Mg^{2+}}$ (mM)	$K_{d,Ca^{2+}}$ (μM)
7a	354, 18.7(1)	328, 17.9(7)	354	328	493, 0.42(1)	483, 0.235(8)	2.7	8.8(4)	64(3)
7b	356, 20.7(7)	323, 17.4(2)	356	323	495, 0.0053(3)	474, 0.080(4)	N.D.	7.8(2)	58.9(8)
7c	356, 21.2(6)	330, 16(1)	356	330	495, 0.42(1)	482, 0.25(2)	2.5	9.5(4)	71(4)
Mag-*mito*	356, N.D.	330, N.D.	356	330	495, N.D.	482, N.D.	2.7	6.7(3)	53.5(9)

[a] Measurements performed in 50 mM PIPES, 100 mM KCl, pH 7.0 at 25 °C. Molar absorptivity coefficients, fluorescence quantum yields and dissociation constants are averages of three determinations; numbers in parenthesis represent the uncertainty on the last significant figure. N.D. = not determined. [b] Quinine sulfate in 0.5 M H_2SO_4 ($\Phi_{347} = 0.546$)[28,29] was employed as a fluorescence standard.

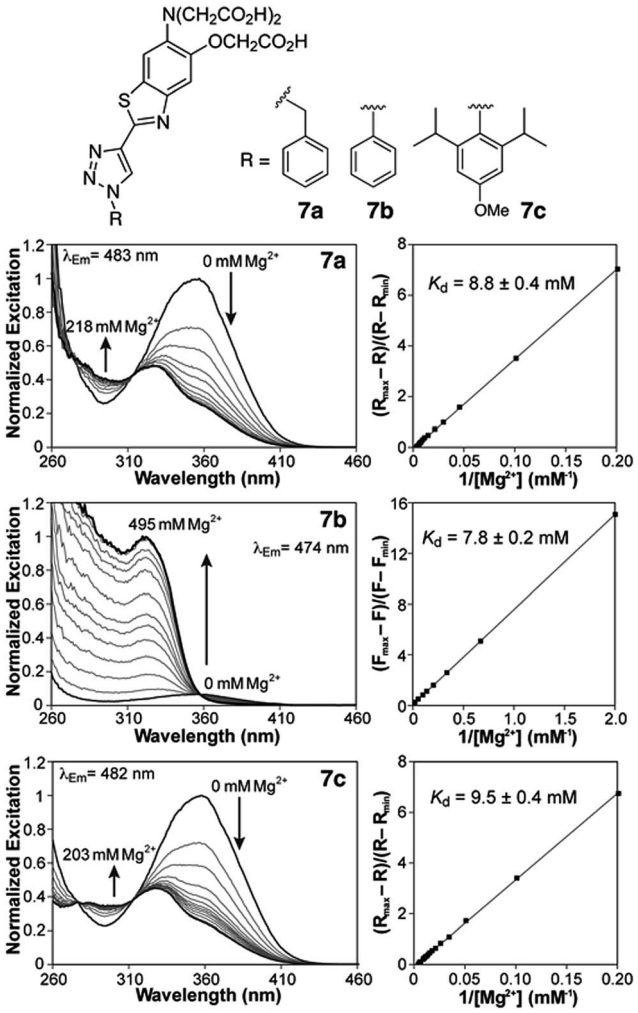

Fig. 2 Fluorescence excitation spectra (left) and double reciprocal plots (right) of 2 μM solutions of compounds **7a**,**c** and 5 μM solution of **7b** with increasing concentrations of $MgCl_2$ (50 mM PIPES, 100 mM KCl, pH 7.0, 25 °C).

new probes is comparable to that of other related *o*-aminophenol-*N*,*N*,*O*-triacetic acid (APTRA)-based metal ion indicators.[23,31] In addition to Mg^{2+}, the compounds respond to mid-micromolar concentrations of Ca^{2+} (Table 1), thus could be employed as low-affinity Ca^{2+} indicators for the study of systems with particularly high concentrations of this ion. For compounds **7a** and **7c**, the changes in spectral properties upon Ca^{2+} coordination are similar to those observed in the presence of Mg^{2+} (Fig. S9 and S11†). For **7b**, on the other hand, binding of Ca^{2+} leads to a blue shift in excitation with no significant increase in the emission efficiency, *i.e.* no turn-on response is obtained (Fig. S10†). The compounds also respond to the micromolar concentrations of Zn^{2+} tested.[32] With few exceptions, however, the typical sub-nanomolar intracellular concentrations of this ion should not interfere with Mg^{2+} detection.[33] Finally, the sensors are insensitive to variations in pH in the 5.5 to 8.0 range (Fig. S13†).

Targeted, organelle-specific sensing of free Mg^{2+}

With insight gained from the model compounds characterized *in vitro*, we focused on the design of a mitochondria-targeted sensor. Mitochondria are regarded as intracellular reservoirs of Mg^{2+}, and are invoked often as central players in the regulation of Mg^{2+} homeostasis due to their ability to take up and extrude this metal ion in a respiration-dependent manner.[11,34,35] The potential caused by the proton gradient across the mitochondrial membrane can be exploited to direct the accumulation of small-molecules to this organelle. With this feature in mind, a derivative functionalized with a lipophilic cationic alkylphosphonium group[36] (**Mag-*mito***, Scheme 2) was prepared. This targeted sensor shows similar photophysical properties and metal response as those displayed by the analogue compound **7c**, devoid of the targeting moiety (Table 1 and Fig. S4 and S12†).

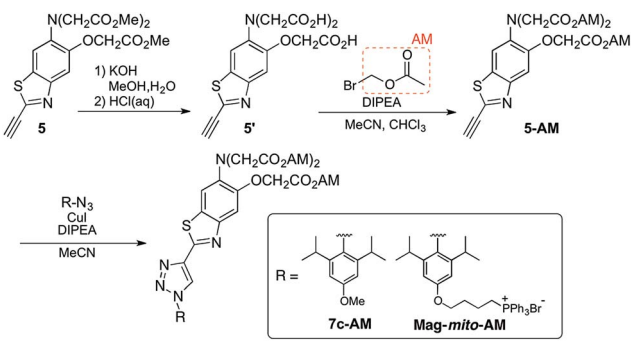

Scheme 2 Assembly of sensors for cellular imaging of Mg^{2+}.

Mag-*mito* was tested for the excitation ratiometric imaging of mitochondrial Mg^{2+} in live HeLa cells by widefield fluorescence microscopy, using filter sets available for Mag-fura-2 and the Ca^{2+}-sensitive analog Fura-2 (Fig. 3). To facilitate cell loading of the compound, the metal-binding carboxylate groups were masked as acetoxymethyl (AM) esters, which are readily cleaved by intracellular esterases after probe uptake.[37] Cells were incubated with 1 μM of the sensor for 30 min at room temperature, rinsed, and then allowed to incubate for another 30 min for full de-esterification of the internalized probe. Successful targeting of the desired organelle was evidenced by a Pearson correlation coefficient of 0.83 in the co-localization analysis with MitoTracker green FM (Molecular Probes, Fig. 3F).[38] This analysis was conducted over the three-dimensional volume of the cell, reconstructed from a *z*-stacked series of images (Fig. S14†). To the best of our knowledge, this is the first example of targeted ratiometric detection of mitochondrial Mg^{2+} with a fluorescent probe.[39] For comparison, the non-targeted analog **7c**, devoid of the alkylphosphonium group, was tested under the same conditions. This sensor showed relatively unselective staining of various compartments (Fig. 3H–J), with a correlation coefficient of 0.55 for the co-localization analysis with the reference mitochondrial stain. The ability of the indicators to respond to changes in intracellular Mg^{2+} concentrations was confirmed by collecting two sets of images of cells stained with non-targeted compound **7c**, before and after treatment with non-fluorescent ionophore 4-bromo-A-23187 (Molecular Probes) and 20 mM of $MgCl_2$ for 60 min. An increase in the average fluorescence ratio per cell (~20%, Fig. 4 and S15†) was observed in response to the increase in intracellular free Mg^{2+} concentration mediated by the ionophore. Furthermore, the fluorescence excitation spectrum of **7c**-loaded HeLa cells treated with ionophore and 50 mM EDTA for 30 min was acquired on a plate reader, showing a red-shift consistent with decreasing concentrations of intracellular Mg^{2+} (Fig. S16†).

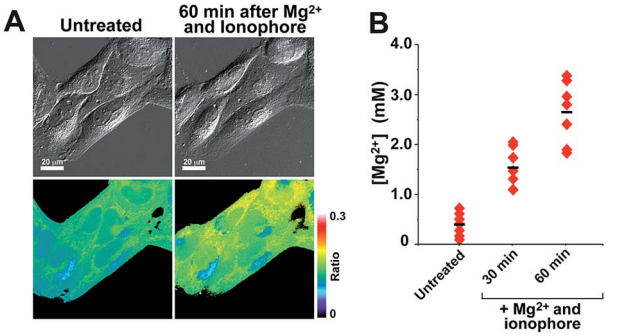

Fig. 4 (A) Fluorescence microscopy images of live HeLa cells treated with 1 μM of compound **7c-AM**, before and after treatment with 2.5 μM Mg^{2+} ionophore 4-bromo-A-23187 and 20 mM exogenous $MgCl_2$. For each set of images (top) DIC images; (bottom) fluorescence ratio images. (B) Average intracellular free Mg^{2+} concentration per cell before and after treatment with exogenous Mg^{2+} and ionophore, calculated from the fluorescence ratio.

Mitochondrial changes in free Mg^{2+} during apoptosis

With a probe capable of detecting free Mg^{2+} in mitochondria, we investigated the changes in ion levels in these organelles during apoptosis induced by Staurosporine (STS) in HeLa cells. Live cells pre-loaded with **Mag-*mito*** were treated with 1 μM of the alkaloid on the fluorescence microscope stage, and monitored over the course of 120 min (Fig. 5). MitoTracker green was employed to confirm the localization of the Mg^{2+} probe and a caspase indicator was used to verify apoptosis, whereas ethidium homodimer-1 was used to rule out possible cell lysis from necrosis. Changes in the fluorescence ratio of the sensor revealed a roughly threefold increase in concentration of free Mg^{2+}, which plateaued at 2.6 mM within 10 min and decreased slowly after ~25 min as the process continued (Fig. 5B). Signal of the sensor and MitoTracker started to appear diffuse after approximately 40 min of observation, likely due to dye leakage upon depolarization of the mitochondrial membrane that makes the estimation of ion concentration less reliable at later

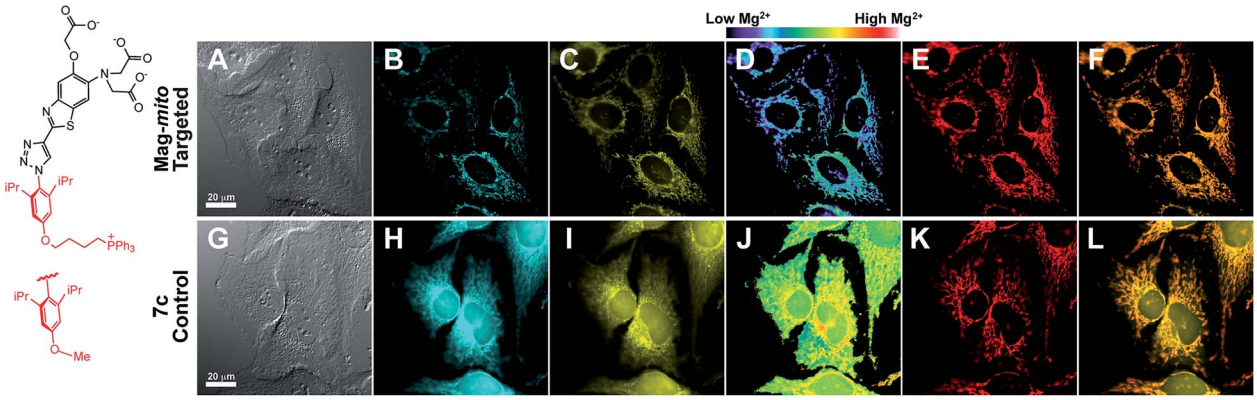

Fig. 3 Widefield fluorescence imaging of intracellular free Mg^{2+} in HeLa cells treated with 1 μM of mitochondria-targeting **Mag-*mito*** (A–F) or untargeted control, **7c** (G–L) in their acetoxymethyl ester form. (A and G) DIC images; (B and H) fluorescence upon excitation at 340 nm; (C and I) fluorescence upon excitation at 380 nm; (D and J) fluorescence ratio 340/380 nm; (E and K) MitoTracker green pseudo-colored in red; (F and L) overlay of 380 nm channel and mitochondrial staining images.

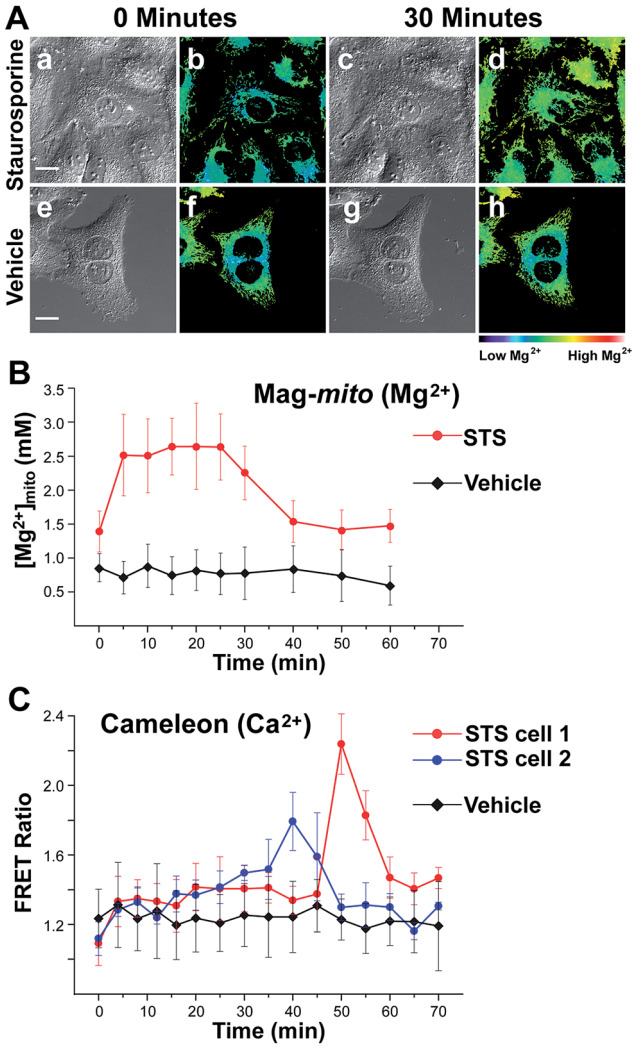

Fig. 5 (A) Widefield fluorescence imaging of mitochondrial free Mg^{2+} in live HeLa cells treated with 1 μM **Mag-*mito*** and with 1 μM apoptosis-inducing Staurosporine (a–d), or vehicle (e–h). Scale bar = 20 μm. (a, c, e and g) DIC images; (b, d, f and h) fluorescence ratio. (B) Changes in mitochondrial free Mg^{2+} in Staurosporine-treated (circles) or vehicle-treated (diamonds) HeLa cells, calculated from changes in fluorescence ratio of **Mag-*mito***. (C) Changes in FRET ratio over time due to changes in free Ca^{2+} in Staurosporine-treated (blue and red circles) and control (black diamonds) HeLa cells transiently expressing cameleon 4mtD3cpv. Blue and red circles correspond to data from mitochondria clusters in different cells, showing asynchronous Ca^{2+} elevations that peaked at different times. Error bars represent standard deviations.

points. Morphological changes associated with apoptosis such as mitochondrial fragmentation and cell blebbing were also observed. The caspase indicator became activated after ~90 min, revealing the downstream events of the apoptosis cascade (Fig. S17†). For comparison, no significant changes were observed in cells treated with vehicle over the same period of time, showing a basal mitochondrial level of 0.8 mM free Mg^{2+} that remained constant throughout the experiment.

Given the weak Ca^{2+} binding ability of APTRA-based sensors, we sought to rule out possible Ca^{2+}-induced signal in our experiment by comparing the fluorescence response of **Mag-*mito*** with that obtained with a genetically encoded Ca^{2+}-specific indicator. We conducted a similar experiment with HeLa cells transiently expressing cameleon 4mtD3cpv, which has been optimized for the detection of Ca^{2+} in mitochondria.[40] The protein-based FRET indicator revealed Ca^{2+} elevations in mitochondria clusters starting after 30–40 min of treatment with the drug (Fig. 5C). The clear differences in the onset and duration of the Ca^{2+} signal in comparison with the response obtained by **Mag-*mito*** are consistent with the detection of Mg^{2+}, and not Ca^{2+}, by the small molecule probe. Another control experiment was conducted by adding tris-(2-pyridylmethyl) amine (TPA), a rapid picomolar Zn^{2+} chelator,[41] 15 min after induction of apoptosis. The fluorescence ratio did not show a decrease within the typical response time of the chelator, ruling out the interference of Zn^{2+} in our measurement (Fig. S18†). To the best of our knowledge, these results represent the first direct observation of changes in mitochondrial free Mg^{2+} during programmed cell death. The source of this pool of free Mg^{2+} is unknown at this time, but it could be attributed to its release from bound forms abundant in the mitochondrion (*e.g.* MgATP), or to an extra-mitochondrial origin. Significantly, studies conducted with isolated mitochondria by Martinou and coworkers have shown that Mg^{2+} may potentiate the release of cytochrome *c* from these organelles,[42] thus hinting to the possible relevance of an early increase in free Mg^{2+} in the apoptotic cascade.

Conclusions

The ability to study metal compartmentalization and mobilization in cells in the context of physiological and pathological processes depends on the availability of fluorescence indicators that enable rapid detection of the ions with subcellular resolution. We have designed a new family of triazole-based fluorescent probes for targeted ratiometric detection of Mg^{2+} in intracellular organelles by fluorescence microscopy. The sensors are rapidly assembled by copper catalyzed alkyne–azide cycloaddition between an alkynyl benzothiazole, functionalized with an APTRA Mg^{2+} recognition unit, and an azide-functionalized organelle-targeting group of choice. The resulting triazole moiety plays both structural and electronic roles in the new sensors, by serving as an attachment group to organelle-targeting moieties and participating in a possible ICT process useful for ion sensing. With appropriate changes to the metal-binding functionality, the sensor design presented herein may be adapted for the targeted detection of other cations of biological relevance.

We developed a sensor functionalized with a lipophilic cationic alkylphosphonium group, *i.e.* **Mag-*mito***, which displays selective localization in mitochondria thus enabling the targeted ratiometric imaging of free Mg^{2+} within these organelles in live cells. A time-course fluorescence imaging study conducted on HeLa cells treated with Staurosporine provided the first direct observation of an increase in free Mg^{2+} levels in mitochondria during early stages of apoptosis. The onset of this change appears to precede Ca^{2+} entry into the

organelle. Future studies will be aimed at identifying the origin and destination of this mitochondrial pool of free Mg^{2+} and its influence in the downstream events in the apoptotic cascade.

Acknowledgements

This research was supported by start-up funds granted to D. B. by New York University. The Bruker Avance-400 NMR spectrometer was acquired through the support of the National Science Foundation under Award Number CHE-01162222. pcDNA-4mtD3cpv was a gift from Amy Palmer & Roger Tsien (Addgene plasmid # 36324).

References

1 J. A. Cowan, in *The Biological Chemistry of Magnesium*, ed. J. A. Cowan, VCH Publishers, New York, 1995, pp. 1–23.
2 F.-Y. Li, B. Chaigne-Delalande, C. Kanellopoulou, J. C. Davis, H. F. Matthews, D. C. Douek, J. I. Cohen, G. Uzel, H. C. Su and M. J. Lenardo, *Nature*, 2011, **475**, 471–476.
3 R. D. Grubbs, *Biometals*, 2002, **15**, 251–259.
4 A. M. P. Romani, *Arch. Biochem. Biophys.*, 2011, **512**, 1–23.
5 N.-E. L. Saris, E. Mervaala, H. Karppanen, J. A. Khawaja and A. Lewenstam, *Clin. Chim. Acta*, 2000, **294**, 1–26.
6 J. A. M. Maier, *Mol. Aspects Med.*, 2003, **24**, 137–146.
7 M. Barbagallo and L. J. Dominguez, *Arch. Biochem. Biophys.*, 2007, **458**, 40–47.
8 T. Hashimoto, K. Nishi, J. Nagasao, S. Tsuji and K. Oyanagi, *Brain Res.*, 2008, **1197**, 143–151.
9 A. M. P. Romani, in *Interrelations between Essential Metal Ions and Human Diseases*, ed. A. Sigel, H. Sigel and R. K. O. Sigel, Springer Netherlands, 2013, vol. 13, ch. 3, pp. 49–79.
10 For reviews of recent advances in magnesium detection with fluorescent indicators, see: (*a*) V. Trapani, M. Schweigel-Roentgen, A. Cittadini and F. I. Wolf, *Methods Enzymol.*, 2012, **505**, 421–444; (*b*) V. Trapani, G. Farruggia, C. Marraccini, S. Iotti, A. Cittadini and F. I. Wolf, *Analyst*, 2010, **135**, 1855–1866.
11 Y. Shindo, T. Fujii, H. Komatsu, D. Citterio, K. Hotta, K. Suzuki and K. Oka, *PLoS One*, 2011, **6**, e23684.
12 T. Fujii, Y. Shindo, K. Hotta, D. Citterio, S. Nishiyama, K. Suzuki and K. Oka, *J. Am. Chem. Soc.*, 2014, **136**, 2374–2381.
13 L. H. Lindenburg, J. L. Vinkenborg, J. Oortwijn, S. J. A. Aper and M. Merkx, *PLoS One*, 2013, **8**, e82009.
14 S. Orrenius, B. Zhivotovsky and P. Nicotera, *Nat. Rev. Mol. Cell Biol.*, 2003, **4**, 552–565.
15 R. Rizzuto, P. Pinton, D. Ferrari, M. Chami, G. Szabadkai, P. J. Magalhães, F. D. Virgilio and T. Pozzan, *Oncogene*, 2003, **22**, 8619–8627.
16 P. Pinton, C. Giorgi, R. Siviero, E. Zecchini and R. Rizzuto, *Oncogene*, 2008, **27**, 6407–6418.
17 T. Patel, S. F. Bronk and G. J. Gores, *J. Clin. Invest.*, 1994, **94**, 2183–2192.
18 X.-Y. Zhang, W.-G. Li, Y.-J. Wu, D.-C. Bai and N.-F. Liu, *Can. J. Physiol. Pharmacol.*, 2005, **83**, 309–318.
19 M. M. Chien, K. E. Zahradka, M. K. Newell and J. H. Freed, *J. Biol. Chem.*, 1999, **274**, 7059–7066.
20 M. Meldal and C. W. Tornøe, *Chem. Rev.*, 2008, **108**, 2952–3015.
21 For examples of triazole-containing molecules in sensing, see: M. Watkinson, in *Click Triazoles*, ed. J. Košmrlj, Springer Berlin Heidelberg, 2012, pp. 109–136.
22 B. Raju, E. Murphy, L. A. Levy, R. D. Hall and R. E. London, *Am. J. Physiol.: Cell Physiol.*, 1989, **256**, C540–C548.
23 R. P. Haugland, *Handbook of Fluorescent Probes and Research Products*, Molecular Probes Inc., Eugene, Oregon, 9th edn, 2002.
24 B. Metten, M. Smet, N. Boens and W. Dehaen, *Synthesis*, 2005, **2005**, 1838–1844.
25 B. Valeur and I. Leray, *Coord. Chem. Rev.*, 2000, **205**, 3–40.
26 H. L. Kee, C. Kirmaier, L. Yu, P. Thamyongkit, W. J. Youngblood, M. E. Calder, L. Ramos, B. C. Noll, D. F. Bocian, W. R. Scheidt, R. R. Birge, J. S. Lindsey and D. Holten, *J. Phys. Chem. B*, 2005, **109**, 20433–20443.
27 Z. R. Grabowski, K. Rotkiewicz and W. Rettig, *Chem. Rev.*, 2003, **103**, 3899–4032.
28 W. H. Melhuish, *J. Phys. Chem.*, 1961, **65**, 229–235.
29 A. M. Brouwer, *Pure Appl. Chem.*, 2011, **83**, 2213–2228.
30 R. K. Gupta, P. Gupta, W. D. Yushok and Z. B. Rose, *Biochem. Biophys. Res. Commun.*, 1983, **117**, 210–216.
31 M. S. Afzal, J.-P. Pitteloud and D. Buccella, *Chem. Commun.*, 2014, **50**, 11358–11361.
32 The related Mag-fura-2 sensor responds to Zn^{2+} with an apparent dissociation constant of 20 nM. See T. J. B. Simons, *J. Biochem. Biophys. Methods*, 1993, **27**, 25–37.
33 R. A. Colvin, W. R. Holmes, C. P. Fontaine and W. Maret, *Metallomics*, 2010, **2**, 306–317.
34 D. W. Jung and G. P. Brierley, *J. Bioenerg. Biomembr.*, 1994, **26**, 527–535.
35 T. Kubota, Y. Shindo, K. Tokuno, H. Komatsu, H. Ogawa, S. Kudo, Y. Kitamura, K. Suzuki and K. Oka, *Biochim. Biophys. Acta, Mol. Cell Res.*, 2005, **1744**, 19–28.
36 B. C. Dickinson, D. Srikun and C. J. Chang, *Curr. Opin. Chem. Biol.*, 2010, **14**, 50–56.
37 R. Y. Tsien, *Nature*, 1981, **290**, 527–528.
38 S. Bolte and F. P. Cordelières, *J. Microsc.*, 2006, **224**, 213–232.
39 The only other instances of selective detection of magnesium in mitochondria in live cells have been reported by the group of Oka and coworkers with KMG-301 and KMG-104-AsH, both intensity-based turn-on probes. See ref. 11 and 12.
40 A. E. Palmer and R. Y. Tsien, *Nat. Protoc.*, 2006, **1**, 1057–1065.
41 Z. Huang, X.-a. Zhang, M. Bosch, S. J. Smith and S. J. Lippard, *Metallomics*, 2013, **5**, 648–655.
42 R. Eskes, B. Antonsson, A. Osen-Sand, S. Montessuit, C. Richter, R. Sadoul, G. Mazzei, A. Nichols and J.-C. Martinou, *J. Cell Biol.*, 1998, **143**, 217–224.

